Supplemental Information

Benjamin Kerr, Claudia Neuhauser, Brendan Bohannan and Antony Dean

(SI for *Local migration promotes competitive restraint in a host-pathogen 'tragedy of the commons'*)

Overview:

In this document we provide the full details of our experimental and theoretical methods and results. We have divided this supplement into five sections. Section I (**Supplemental Methods**) focuses on experimental protocol, the derivation of mathematical quantities used in laboratory assays, and statistical analysis of experimental data. Section II (**The Evidence for Phage Evolution**) describes the observations that led us to propose that evolution of phage had occurred. Section III (**Configuration Field Approximation**) outlines an analytical approach to predicting metapopulation dynamics and compares this approach to stochastic cellular automata. Section IV (**Small Lattice Simulations**) explores the behavior of simulated metapopulations that are built to match the size of our experimental metapopulations exactly, which allows us to choose parameter settings for the experiment and make more specific predictions that take into account demographic stochasticity. Section V (**Evolutionary Model**) builds on section III and the Box to include the evolution of phage strategies within the modeling framework.

Contents:

I. *Supplemental Methods*

Section Overview:

In this section we spell out all of our methods in detail, including a recipe list, a full description of and rationale behind the experimental approach, some supporting protocols, mathematical derivation of useful quantities (such as competition indices and number of microbial generations) and statistical analysis and results.

Media recipes:

1) **Growth Media**:

Potassium Phosphate Dibasic	7g
Potassium Phosphate Monobasic	2g
Ammonium Sulfate	1g
10% Glucose Solution	10mL
10% Magnesium Sulfate	1mL
0.2% Thiamine	1mL
100mg/mL Streptomycin	1mL
100mg/mL Novobiocin	1mL
Distilled water	1000mL

The growth media filling the microtitre plates (used in the experimental runs and the assays) was the minimal glucose recipe given above. The streptomycin was added to prevent contamination and the novobiocin was added to limit the generation of T4 resistant bacterial mutants (although we did detect T4-resistant bacteria towards the end of the experiment).

2) **LB hard agar**:

Tryptone	10g
Yeast Extract	5g
Sodium Chloride	10g
Agar	15g
Distilled water	1000mL

Counting of both bacteria and phage was done on LB agar plates.

3) **LB soft agar (SIB soft agar)**:

Tryptone	10g
Yeast Extract	5g
Sodium Chloride	10g
Agar	10g
Distilled water	1000mL

SIB soft agar was used as an overlay on the LB agar base (for counting phage).

4) **PEG6000 Solution (20%)**

PEG6000	20g
Sodium Chloride	14.6g
Distilled water	100mL

The PEG6000 solution was used to concentrate phage (see below).

5) **Saline Solution (0.86%)**

Sodium Chloride	8.6g
Distilled water	1000mL

All dilutions (of bacteria and phage) took place in the above saline solution.

6) **TA agar**:

Tryptone	10g
Yeast Extract	1g
Sodium Chloride	5g
Agar	16g
Arabinose	10g
2,3,5 Triphenyl Tetrazolium Chloride (5%)	1mL
Distilled water	1000mL

TA plates were used for counting bacteria colonies in the bacterial competitions.

Contamination prevention:

We had to contend with two sources of contamination in this experiment: contamination from outside the experiment and contamination from within the experiment. The antibiotics streptomycin and novobiocin were added to prevent outside contamination. Also, we removed sodium citrate from the standard minimal glucose medium as we discovered a contaminant that was able to use citrate as a carbon source in a pilot run. We also were concerned with cross-well contamination (inappropriate migration within the microtitre plate). To prevent such within-experiment contamination, all microtitre plates were covered with a Breathe-Easy strip during shaking. Several pilot runs with these strips demonstrated their effectiveness in preventing spill-over between wells.

Experimental metapopulations:

For every transfer cycle, each metapopulation replicate (two 96 well plates) was incubated at 37°C and shaken at 550rpm on a microtitre shaker for about 10.5 hours (the robot transfer itself took about an hour and a half). The volume of growth media in every well was maintained at 200μL. As shown in Figure SI.1, in the Restricted and Unrestricted treatments each well was diluted tenfold into the corresponding well in plates with fresh growth media. And this dilution was followed immediately by migration. Therefore, the phage populations experienced their hosts in a 'burst' every 12 hours rather than in a steady 'stream'. The evolution of phage strategies in our experiment may be influenced by such periodic growth (e.g., there could be selection for phage mixed with bacteria at low multiplicity of infection to time its lysis for optimal later use of the uninfected and growing portion of the bacterial population). Overall, our results might be

most applicable to host-pathogen systems in which discrete bursts of death and migration occur within the metapopulation (although our results are consistent with some predictions from continuous time theory—e.g., Keeling 2000).

After dilution, a migration event occurred into the new focal well with probability m=0.45. In the Restricted treatment, the source of this migration was one of the north, south, east or west neighbouring wells, diluted from the spent media plates approximately tenfold into the new focal well. In the Unrestricted treatment, the neighbourhood around a focal well included the entire collection of wells, minus the focal. In the Well-Mixed treatment, all wells were diluted tenfold into a common reservoir with fresh growth media, the reservoir was physically mixed, and the mixture was dispensed into wells of two empty plates.

Figure SI.1

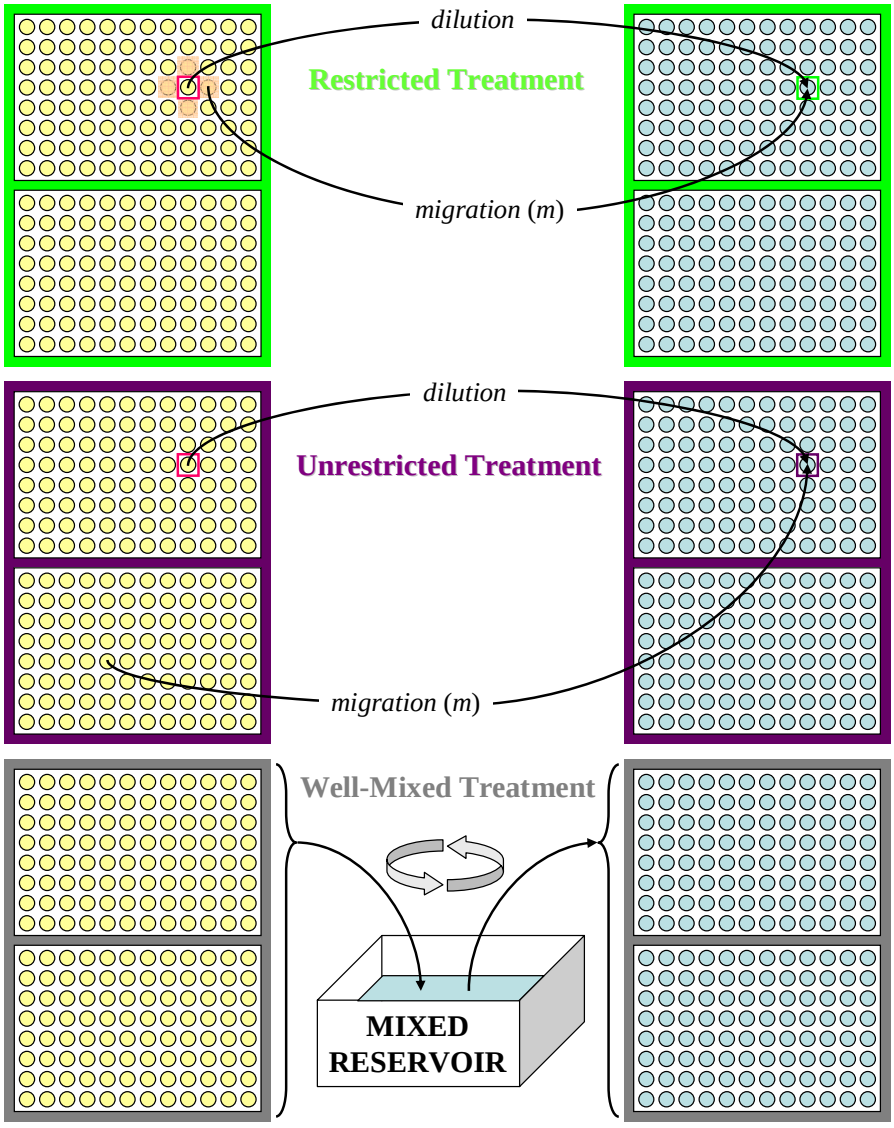

A transfer event is shown for the three treatments. Like the 'example focal well' (boxed in bright pink), each well in the Restricted treatment is diluted from spent media (yellow) into fresh media (blue). Then, with probability m=0.45, migration occurs from one of the four nearest wells (highlighted in pink) into the focal well. The Unrestricted treatment is identical except that any well in the metapopulation can serve as the migration source. In the Well-Mixed treatment, all wells are diluted into a common reservoir, thoroughly mixed, and redistributed into a fresh set of wells.

The multichannel pod of the Biomek FX performed the dilution portion of the metapopulation transfer (96 wells diluted at once in each case). A program (written in C) generated text files that gave the source and destination well of every migration event for every transfer (generated randomly according to the migration probability). The function 'WorkList' in the robot's software was used to loop through all of these migratory events using the Span-8 pod.

The robot was also used for the Well-Mixed treatment. Here the contents from every well in the spent media plates were dispensed (in a tenfold dilution) into a reservoir with fresh growth media using the multichannel pod. This reservoir was physically mixed and then the robot dispensed 200μL of the mixture into each well of two empty plates (which became the next transfer's metapopulation to be incubated/shaken).

Bacteria and phage rapidly disappeared from the Well-Mixed metapopulations. We ended the Well-Mixed runs after five consecutive transfers in which no bacteria or phage could be detected. One of the Unrestricted replicates had to be terminated early (transfer 16) because of contamination. The rest of the metapopulations were run for 20 transfers.

Isolating evolved phage:

We plated out a dilution of each Restricted and Unrestricted replicate from the last transfer of the experiment so that individual plaques could be picked. We used K-12 λ-lysogen cells to isolate the phage that were not rII mutants. This 'rapid lysis' rII mutant will not form plaques on K-12 λ-lysogen host cells. A good fraction of the evolved phage from the last transfer was rII (but this fraction did not differ significantly with migration treatment, see Figure SII.2). We isolated four plaques at random by placing a 262 point hexagonal grid under the overlay plate and using a random number generator to pick four points. The plaques closest to the random numbers chosen were isolated, grown on fresh host to amplify their titre, separated from the host cells, and stored for assays in 4°C. Thus, we isolated a total of 32 plaques (2 treatments, 4 replicates/treatment, 4 isolates/replicate). The random picking procedure was implemented to prevent bias in the selection of plaques from different treatments.

Estimating bacterial and phage densities:

At every metapopulation transfer, samples from all wells in the replicate were diluted tenfold into a reservoir filled with saline. Moving very quickly (so as to limit the amount of phage infection), the reservoir was physically mixed and diluted in saline to an appropriate concentration for plating. To estimate bacterial densities, a 100μL aliquot of the appropriate dilution of the mixture was plated on LB. After 24 hours of incubation at 37°C, we counted the number of colonies to give the bacterial count. To estimate the phage densities, a 100μL aliquot of the appropriate dilution of the mixture was combined with 300μL of fully grown REL606 culture into 3mL of SIB soft agar and spread over a hard LB agar base. After 24 hours of incubation at 37°C, we counted the number of plaques to give the phage count.

For the productivity assay, phage counts were obtained by the same soft agar overlay technique both before and after the 12 hour incubation period. For the competition assay, the mixture of evolved T4 phage and rII phage was plated twice in a soft agar overlay, both before and after the 12 hour incubation period. The first overlay used REL606 as the host and the second overlay used K-12 λ lysogen as the host. Since REL606 is sensitive to both evolved T4 and rII, but K-12 λ lysogen is sensitive to evolved T4 and resistant to rII, we can estimate both phage densities (evolved T4 by counting plaques on the K-12 plate and rII by subtraction).

Increasing phage titres:

Sometimes the phage concentration was too low to achieve the appropriate multiplicity of infection for a productivity or competition assay. To concentrate the phage, we employed the following procedure:

1) Placed 1mL of phage and 0.6mL of PEG6000 solution in a 1.5mL epi tube
2) Vortex this tube and let it sit on ice for 1½ hours
3) Spin tubes at 12,000g at 4°C for 10 minutes
4) Discard supernatant and add 30μL of saline solution and vortex

Usually, this procedure lifted the concentration of phage about 10-fold.

Derivation of the competitive ability indices:

In what follows, we derive the three measures of competitive ability (or relative fitness) that we use in the phage competition assays. In all cases, $N_i(t)$ denotes population size of type i at time t.

Per transfer

Consider a population with two types of asexual organisms, A and B. Let the frequency of A be given by p and the frequency of B be given by q (where $p+q=1$). Over a period of time of length τ, the following recursions apply:

$$p' = \frac{\omega_A}{\omega_A p + \omega_B q} p = \frac{\omega_A}{\overline{\omega}} p ,$$

$$q' = \frac{\omega_B}{\omega_A p + \omega_B q} q = \frac{\omega_B}{\overline{\omega}} q ,$$

where ω_i is the absolute fitness of strain i over τ and $\overline{\omega}$ is average fitness over τ. Here we assume these ω's are constants (this is not the case for frequency-dependent selection). One measure of fitness (or competitive ability) of strain A relative to strain B is the ratio of their absolute fitnesses:

$$v(A,B) = \frac{\omega_A}{\omega_B} = \frac{p'/p}{q'/q} .$$

We know

$$p = \frac{N_A(0)}{N_A(0) + N_B(0)} ,$$

$$p' = \frac{N_A(\tau)}{N_A(\tau) + N_B(\tau)} ,$$

$$q = \frac{N_B(0)}{N_A(0) + N_B(0)} ,$$

$$q' = \frac{N_B(\tau)}{N_A(\tau) + N_B(\tau)}.$$

Therefore,

$$v(A,B) = \frac{N_A(\tau)/N_A(0)}{N_B(\tau)/N_B(0)}.$$

Per doubling

Imagine that a population of two types of asexual organisms, *A* and *B*, have been reproducing over a period of time τ. If the initial total population size is $N(0)$ and the final population size is $N(\tau)$, then the number of doublings is

$$D = \log_2(N(\tau)/N(0)).$$

Now, for a single doubling period, the following recursion applies:

$$p' = \frac{\upsilon_A}{\upsilon_A p + \upsilon_B q} p = \frac{\upsilon_A}{\bar{\upsilon}} p,$$
$$q' = \frac{\upsilon_B}{\upsilon_A p + \upsilon_B q} q = \frac{\upsilon_B}{\bar{\upsilon}} q,$$

where υ_i is the absolute fitness of strain *i* over a doubling period (all υ's are assumed to be constant—i.e., no frequency dependence). Let $z=p/q$. We have the following recursion for *z*:

$$z' = \frac{\upsilon_A}{\upsilon_B} z,$$

Thus, iteration of the above recursion *D* times gives:

$$z^{(D)} = \left(\frac{\upsilon_A}{\upsilon_B}\right)^D z.$$

One measure of fitness (or competitive ability) of strain *A* relative to strain *B* is the ratio of their absolute fitnesses over the doubling period:

$$u(A,B) = \frac{\upsilon_A}{\upsilon_B} = \sqrt[D]{\frac{z^{(D)}}{z}}.$$

We know

$$z = \frac{N_A(0)}{N_B(0)},$$
$$z^{(D)} = \frac{N_A(\tau)}{N_B(\tau)}.$$

Therefore,

$$u(A,B) = \frac{\sqrt[D]{N_A(\tau)/N_A(0)}}{\sqrt[D]{N_B(\tau)/N_B(0)}}.$$

Assuming continuous exponential growth

A commonly used measure of fitness in microbial studies is the ratio of Malthusian parameters. For strains *A* and *B*, assume exponential growth:

$$N_A(t) = N_A(0)e^{r_A t},$$
$$N_B(t) = N_B(0)e^{r_B t}.$$

One measure of fitness (or competitive ability) of strain *A* relative to strain *B* is the ratio of their Malthusian parameters:

$$w(A,B) = \frac{r_A}{r_B}.$$

Now, consider both strains growing over a finite period τ. If we know the initial and final counts of each strain, then we have $w(A,B)$:

$$w(A,B) = \frac{\ln\left(N_A(\tau)/N_A(0)\right)}{\ln\left(N_B(\tau)/N_B(0)\right)}.$$

Note that all of these measures of fitness are related. Let f_i be the factor by which type *i* increases over the period of time τ (i.e., $f_i = N_i(\tau)/N_i(0)$). Our three measures can be rewritten:

$$v(A,B) = \frac{f_A}{f_B},$$
$$u(A,B) = \frac{(f_A)^{1/D}}{(f_B)^{1/D}},$$

$$w(A,B) = \frac{\ln f_A}{\ln f_B}.$$

If f_A and f_B are both greater than unity, we know

$$f_A > f_B \Leftrightarrow v(A,B) > 1 \Leftrightarrow u(A,B) > 1 \Leftrightarrow w(A,B) > 1,$$
$$f_A < f_B \Leftrightarrow v(A,B) < 1 \Leftrightarrow u(A,B) < 1 \Leftrightarrow w(A,B) < 1,$$

given that $y=x^{1/D}$ and $y=\ln x$ are positive monotonic increasing functions (for $x>1$). Thus, for cases where both types are expanding, a fitness (of *A* relative to *B*) above unity suggests that *A* out-competes *B*, despite the measure used. When $f_i<1$ (the population size of a type shrinks over the period) then the $w(A,B)$ measure can present problems. Specifically, $w(A,B)$ can be negative (e.g., if $f_A<1$ and $f_B>1$) or $f_A < f_B < 1 \Rightarrow w(A,B) > 1$, that is, a type that decreases more dramatically appears to be the better competitor. Of course, all these problems occur because $\ln x<0$ for $0<x<1$. As long as $f>1$, we avoid problems. For our phage competitions, we used all three measures, ignoring the *w* measures when unreasonable. Generally, all three measures yielded similar results.

Bacterial competitions:

Bacterial strain REL607 is identical to our ancestral bacterial REL606 except that 607 is marked with the ability to utilize the sugar arabinose. From the last transfer of our experimental runs we selected three random bacterial isolates from each of the Restricted and Unrestricted replicates (24 in all). These isolates had REL606 as their ancestor and thus shared its arabinose marker (inability to use this sugar). For each competition, we mixed 10μL of REL607 with 10μL of the given bacterial isolate in a well with 180μL growth medium. We measure the density of bacterial cells before and after 12 hours of incubation by plating out appropriate dilutions of the mixed culture on TA agar plates (ara^+ 607 cells produce pink colonies, while ara^- 606 cells produce red colonies). We found no significant differences in bacterial fitness over treatments (see below). We used $w(A,B)$ from the previous section to compute bacterial relative fitness.

Derivation of the number of phage generations:

Let the concentration of phage in a metapopulation at the end of transfer *t* be C_t (PFU/*mL*). After the 10-fold dilution that initializes a new transfer cycle (in which 20μL in each well is transferred to a well with 180μL of fresh medium in the corresponding position on the microtiter plate), the concentration of phage in the new metapopulation will be:

$$C_{t,dil} = 0.1C_t$$

However, we also have migration to consider. The chance that a well receives a migration of 20μL from another well is $m=0.45$. In such a case, we will be combining 200μL with an expected concentration of $C_{t,dil}$ and 20μL of an expected concentration of C_t. Note that for every migration event we discard 20μL from the destination well (after mixing the 20μL from the source well into the destination well) to keep every well at a constant volume of 200μL; however, simply removing volume will not change phage concentration. So, after migration, the concentration of phage is expected to be:

$$C_{t,mig} = 0.55C_{t,dil} + 0.45\left\{\left(\frac{200}{220}\right)C_{t,dil} + \left(\frac{20}{220}\right)C_t\right\},$$

which, after simplifying, gives approximately

$$C_{t,mig} = 0.137C_t .$$

We also measure the concentration of phage at the end of the transfer period (C_{t+1}). Given that volume is maintained constant over the 12 hours of incubation, we have the following (letting D_{t+1} be the number of viral doublings for transfer t+1):

$$C_{t+1} = C_{t,mig}\,2^{D_{t+1}}$$

Solving for D_{t+1} and using the equalities above we have the following:

$$D_{t+1} = \log_2\left[\frac{C_{t+1}}{0.137C_t}\right].$$

This equation allows us to compute D_{t+1} directly from our data (we have C_t for each transfer t). Note that it is possible for the above doubling number to be negative—this can occur when there are sampling errors or if, by chance, a larger than expected number of migrations occur from media-filled wells into wells with phage and few migrations bring bacteria and phage together (in our data, 14 of 156 D values were negative). Given that we would like to avoid negative generation times, we define the number of generations (doublings) as:

$$\tilde{D}_{t+1} = \max(0, D_{t+1})$$

The total number of generations for the entire run of any given replicate is defined to be

$$T = \sum_{t=1}^{20} \tilde{D}_{t+1},$$

except in the case of one replicate from the Unrestricted treatment that was stopped after 16 transfers due to later contamination. For that replicate we measured the properties of phage after 16 transfers, so the appropriate number of generations is

$$T = \sum_{t=1}^{16} \tilde{D}_{t+1}.$$

We find that the treatments (Restricted and Unrestricted) do not differ in the computed generation times (see below). This result does not change if we include negative D values (that is, replace $\tilde{D}_{t+1}$ with D_{t+1}).

Statistical Analyses:

In the paper, we use non-parametric statistical tests. In the following table, we report both these non-parametric statistics as well as the corresponding parametric *p* values (with the exception of intermediate MOI competitive ability and high MOI competitive ability, the non-parametric and parametric tests agree).

	Mann-Whitney Test	***T Test***
Bacterial coefficient of variation	W=3, p= 0.2	p=0.169252
Phage coefficient of variation	W=0, p=0.02857	p=0.008214
Bacterial average density	W=7, p=0.89	p=0.68225
Phage average density	W=4, p=0.34	p=0.1968202
Low MOI productivity	W=183, p=0.03874	p=0.036946
Intermediate MOI productivity	W=195, p=0.01076	p=0.007161
High MOI productivity	W=187, p=0.026	p=0.010348
Low MOI competitive ability	W=57, p=0.00661	p=0.029564
Intermediate MOI competitive ability	W=41, p=0.00065	p=0.286519
High MOI competitive ability	W=70, p=0.0288	p=0.165011
Bacterial fitness	W=84, p=0.5137	p=0.5356227
Number of phage generations	W=8, p=1	p=0.9703

We pooled all the data at each MOI and calculated Kendall's correlation: low MOI τ=–0.25, T=186, p=0.04545; intermediate MOI τ=–0.1411, T=213, p=0.2655; high MOI τ=–0.4355, T=140, p=0.00033.

II. The Evidence for Phage Evolution

Section overview:

In this section, we describe what led us to explore evolution in the pathogen. Specifically, we describe the discovery of plaque and genetic polymorphisms in our phage population.

Plaque polymorphism:

After only a few transfers within the experimental metapopulations, we noticed dramatically different plaque morphologies produced by phage we were counting. In Figure SII.1a, a section of a Petri dish with a soft agar overlay is shown. Each hole is a bacteriophage plaque in a lawn of bacteria (the plaque is produced by the descendants of a single phage particle that use the available bacterial hosts to go through several rounds of lytic reproduction). In Figure SII.1a, we see plaques that are small and cloudy (the ancestral plaque morphology) and other plaques that are large and clear (a novel morphology). Furthermore, if these plaques are isolated and grown with susceptible bacteria and then plated out on another Petri dish, we see that the plaque morphology is inherited. For instance, Figure SII.1b shows plaques produced by phage coming from an isolated large clear plaque from the original plate and Figure SII.1c shows plaques produced by phage coming from an isolated small cloudy plaque from the original plate. Both plaque types are found throughout the entirety of the experiment. This was our first suggestion that the phage population was evolving.

Figure SII.1

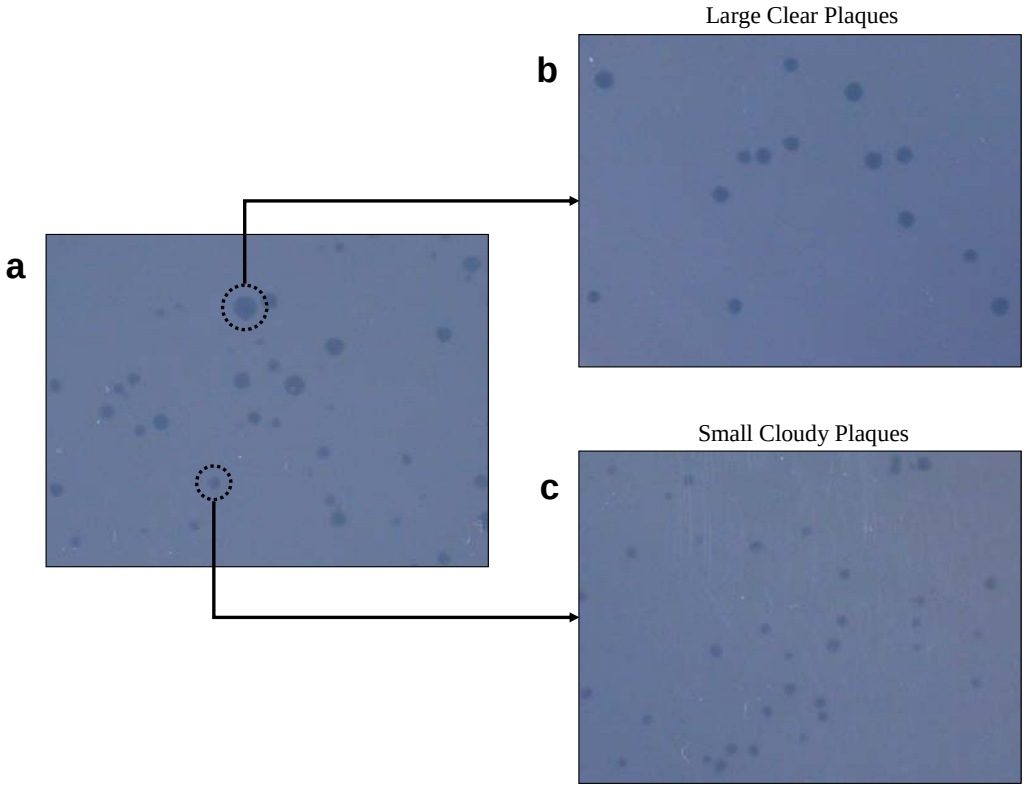

(a) A small section of a Petri dish with phage plaques of two morphologies (large clear plaques and small cloudy plaques). These phage were plated from the second transfer of one of the Restricted migration replicates. When plaques are isolated, they breed true: (b) phage producing large clear plaques continue to do so and (c) phage producing small cloudy plaques continue to do so.

Genetic polymorphism:

We thought that the large clear plaques might be produced by rII mutants (one of several rapid lysis mutants). We quickly discovered that at least some of these large clear plaques were *not* rII mutants (they produced plaques on *E. coli* K-12 λ-lysogen). However, in the process, we discovered that there was a fraction of the phage population that was rII. In Figure SII.2, we track the rII fraction of the phage populations over the course of the experiment. We see that even at the beginning of the experiment a fraction of the phage was rII. Note that we had to grow up phage before the experiment started to have a sufficient volume of concentrated phage to initialize the metapopulations—this pre-experimental growth was apparently sufficient to produce and select for rII mutants.

We see that the fraction of rII mutants increases and levels off at about 65% in both of the two treatments. While we do not detect differences in rII evolution between treatments, these trajectories do give further evidence that the phage population readily evolves in this experimental context. The reasons for this sustained polymorphism in the phage is currently under investigation.

A sizeable rII fraction of the evolved phage population speaks to the relevance of our competition assay. We competed evolved non-rII phage against a common rII competitor. Given the large frequency of rII in the population, this competition is bound to be pertinent to evolving phage.

Figure SII.2

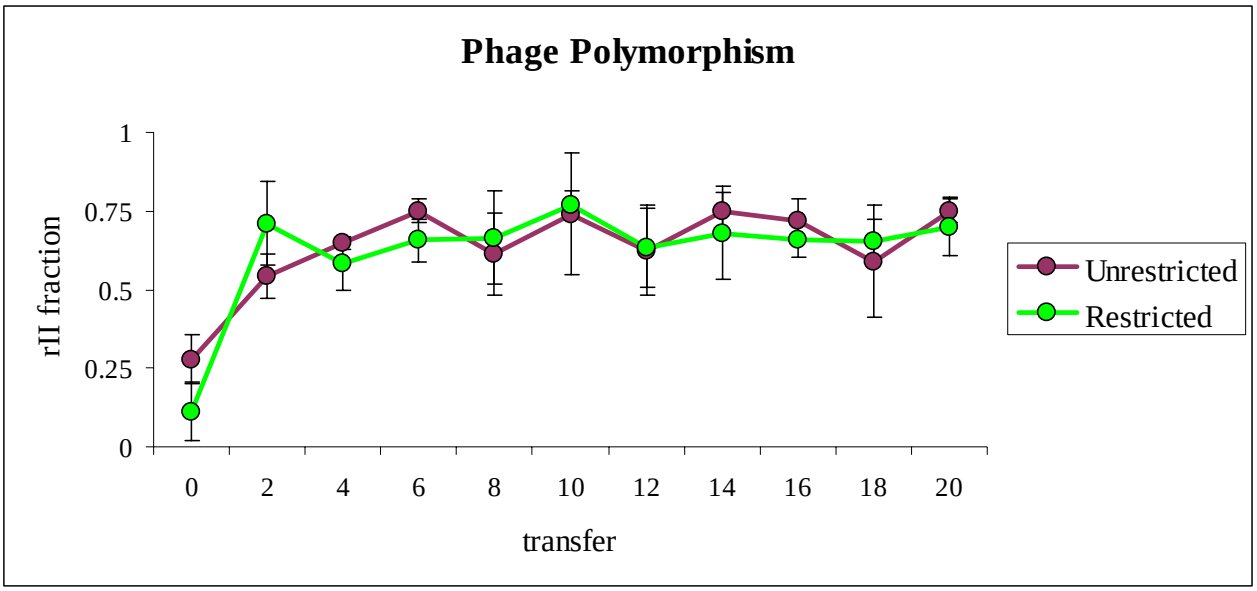

The fraction of rII mutant T4 bacteriophage across the entire experiment. This phage mutant does not produce plaques on *E. coli* K-12 λ-lysogen and this allows us to distinguish this strain from the non-rII evolving phage population.

III. *Configuration Field Approximation*

Section overview:

In this section we outline the configuration field approach, show some numerical results and explain the relationship between the configuration field approximation and stochastic cellular automata with different patterns of migration.

Analytic method:

Imagine an infinite collection of wells, where each well is in one of the states in Table 1. At any point in time we can describe the metapopulation by the vector

$$\mathbf{x}_t = \langle B_t, P1_t, P2_t, P3_t, E_t \rangle,$$

where the ordered quintet gives the frequencies of wells in each of the five states at time *t*. A migration event occurs into any focal well with probability *m*. Conditional on migration, we assume that the probability that the source is in a particular well state is given by that state's frequency (i.e., migration is completely unlimited). The dynamics of **x** are given by

$$\mathbf{x}_{t+1} = \mathbf{x}_t \mathbf{M}_t, \tag{SIII.1}$$

where

$$\mathbf{M}_t = \begin{bmatrix} (1-m)+ & m\begin{Bmatrix} P1_t + \\ P2_t + P3_t \end{Bmatrix} & 0 & 0 & 0 \\ m\{B_t + E_t\} & & & & \\ 0 & mB_t & \begin{matrix}(1-m)+ \\ m\begin{Bmatrix} P1_t + P2_t + \\ P3_t + E_t \end{Bmatrix}\end{matrix} & 0 & 0 \\ 0 & mB_t & mP1_t & \begin{matrix}(1-m)+ \\ m\begin{Bmatrix} P2_t + \\ P3_t + E_t \end{Bmatrix}\end{matrix} & 0 \\ 0 & mB_t & mP1_t & mP2_t & \begin{matrix}(1-m)+ \\ m\{P3_t + E_t\}\end{matrix} \\ mB_t & 0 & mP1_t & mP2_t & \begin{matrix}(1-m)+ \\ m\{P3_t + E_t\}\end{matrix} \end{bmatrix}.$$

One can see the similarity between Table 1 and the stochastic matrix $\mathbf{M}_t$. Note that $\mathbf{M}_t$ is not a constant matrix, but rather depends on the frequencies of well states. The configuration field approximation (Czárán 1998) to the dynamics of our metapopulation of wells is given simply by iteration of the non-linear Markov chain (SIII.1).

Numerical runs:

The configuration field approach predicts that phage should go extinct while bacteria persist if migration between wells is low (see Figure SIII.1a and SIII.1b), whereas both bacteria and phage should coexist at higher migration rates (first at stable levels, then as intermingling

cycles—see Figures SIII.1a, SIII.1c and SIII.1d). In the stochastic cellular automata, the Unrestricted neighbourhood should behave similarly to the configuration field approximation when the lattice size is large (as we see in Figure SIII.1e). The Restricted neighbourhood stochastic cellular automaton allows exploration of a more structured metapopulation and its dynamics can deviate dramatically from the configuration field approximation (see Figure SIII.1f).

Figure SIII.1

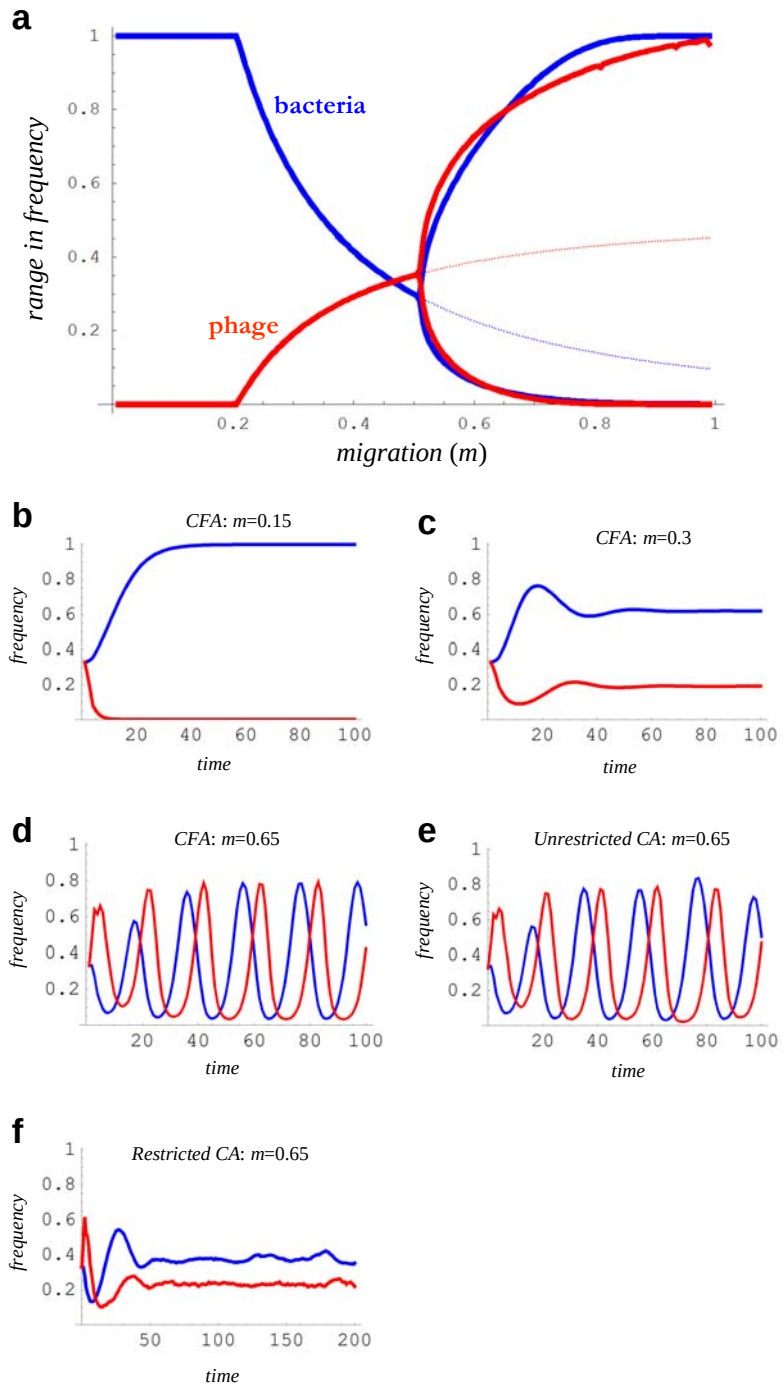

(a) A bifurcation diagram giving the maximum and minimum frequencies of wells filled with bacteria (blue) and phage (red) as a function of migration between wells. We use a configuration field approximation and collect all three phage concentrations into a single trajectory. The unstable internal equilibria that appear after the bifurcation (a little above m=0.5) are given by the dotted lines. For low migration rates, the phage cannot coexist with the bacteria (an example dynamic is given in b). As the rate of inter-well migration is increased, phage and bacteria coexist, first as stable equilibria (an example dynamic is given in c) then as intermingling cycles (an example dynamic is given in d). (e) The Unrestricted stochastic cellular automaton gives dynamics very similar to that predicted by the configuration field approximation, whereas (f) the Restricted automaton possesses distinct dynamics.

IV. *Small Lattice Simulations*

Section overview:

In order to (1) choose a migration rate for the experimental runs, (2) establish initial spatial arrangement of well-states in the metapopulations, and (3) make predictions about metapopulation behaviour, we needed to run simulations (stochastic cellular automata) with lattices that matched the size of the metapopulations used in the experiment. The experimental metapopulations were composed of two 96-well plates (each with dimensions 8×12). Designating one microtitre plate as 'Top' and the other plate as 'Bottom', the two plates were arranged so that the bottom row of 12 wells in the Top plate 'bordered' the top row of 12 wells in the Bottom plate (thus giving a metapopulation of 192 wells with dimensions 16×12). In this section, we will refer to this as the 'small lattice' (a 192 point lattice with dimensions 16×12). In both the simulated and experimental metapopulations, we employed 'wrap around' boundaries so that every well had four nearest neighbours (this was only relevant for the Restricted neighbourhood simulations).

Choosing a migration rate:

Given that we have a small lattice, there is the possibility of stochastic loss of bacteria and/or phage from our metapopulation. Because the migration rate strongly influences the nature of the community dynamics, the migration rate will influence the likelihood of stochastic loss. Consequently, we must select the migration rate with care. Using the well-state transition matrix in Table 1, we run both Unrestricted and Restricted neighbourhood cellular automata with a variety of migration probabilities. We restrict migration to the range required for coexistence within the configuration field approximation (Figure SIII.1a), namely, m must be larger than approximately 0.2. The dynamics for m=0.3, m=0.45, and m=0.6 are shown in Figure SIV.1.

Figure SIV.1: Small Lattice Dynamics

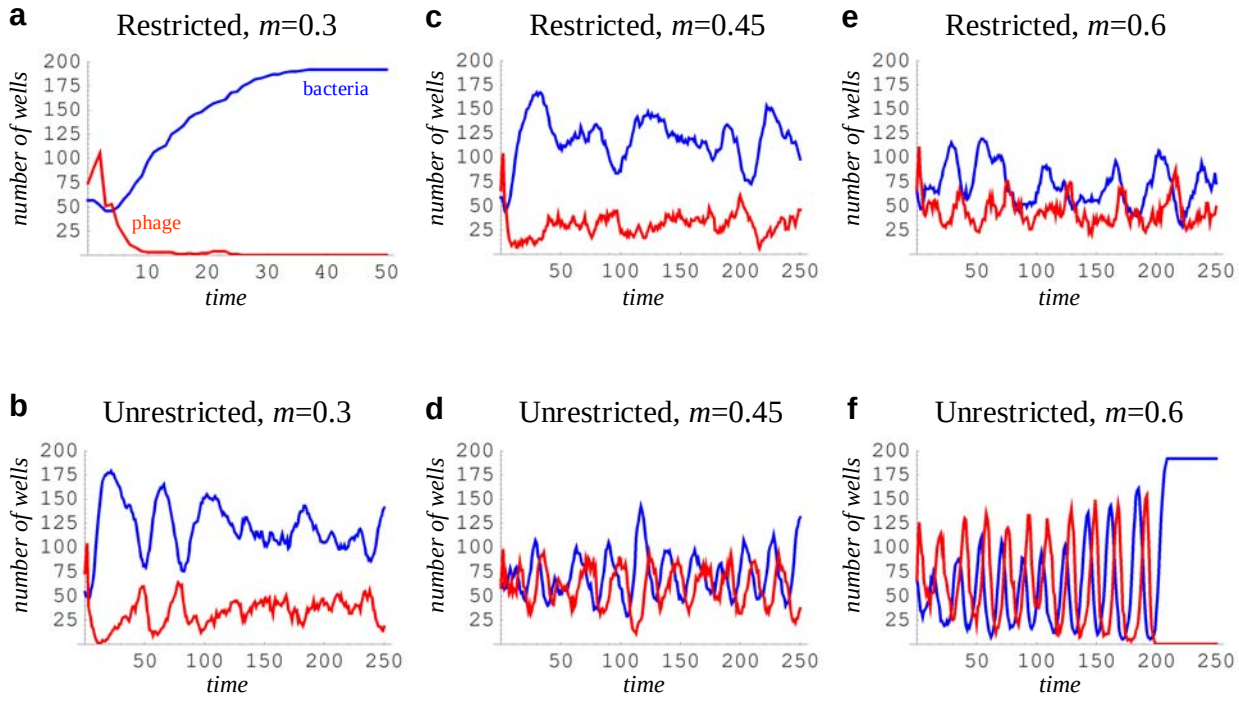

Even if migration is within the range allowing coexistence in the configuration field approximation, phage in the Restricted neighbourhood cellular automaton will not persist if migration is too low (e.g., Figure SIV.1a). This is because of the limit to host access imposed by the Restricted migration scheme. If migration is too high, then there can be extinction in the Unrestricted neighborhood (e.g., Figure SIV.1f). This is because the simulated lattice is *small* (the configuration field approach assumes an *infinite* metapopulation) and relatively large fluctuations occur with a high migration rate, making an extinction event likely. For intermediate migration levels, phage and bacteria persist in both the Restricted and Unrestricted schemes (e.g., Figure SIV.1c and Figure SIV.1d). Because we wanted to avoid both host-limited extinctions and stochastic extinctions, we decided to run all of our experiments at an intermediate migration rate (we chose m=0.45).

Notice that the Unrestricted dynamics in Figures SIV.1b, SIV.1d, and SIV.1f do not correspond exactly to the dynamic behaviour predicted by the configuration field approach. Specifically, we see cyclic behavior for migration values where stable dynamics are predicted (e.g., Figure SIV.1d where m=0.45). This is due to the finite nature of the small lattice. It is as if the community is 'trying' to cycle into a stable internal node, but keeps getting knocked off of this approach by stochastic demographic events. The result is continued cycles (and we see these cycles in our experimental runs as well). Fixing the migration probability at m=0.45, we note a few differences between the Restricted and Unrestricted simulations. First, the Restricted dynamics are more stable (see below). Second, the mean phage density is lower in the Restricted simulation. Third, the mean bacterial density is higher in the Restricted simulation.

Initial spatial configuration:

Figure SIV.2: Initial Well Arrangement

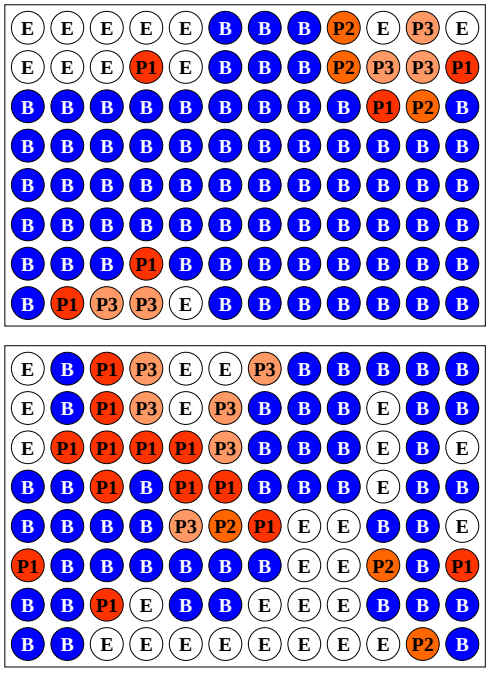

In simulations on large lattices with random initial spatial configurations, there was pronounced transient behaviour in the dynamics of the Restricted neighbourhood simulation (see Figure 1b). The transient behaviour is due to the fact that the metapopulation does not start out spatially clumped; as this clumping develops, the dynamics stabilize. We wanted to avoid this transient, so we pursued the following strategy: We performed a single lattice-based simulation on the small lattice with a Restricted neighbourhood (see Box). After 2000 update steps, we recorded the spatial arrangement of wells in the small lattice and used this spatial arrangement for our initial spatial distribution in all experimental treatments. Figure SIV.2 shows the actual initial distribution of well-states, with bacteria wells in blue, phage wells in shades of red, and empty wells in white (117 **B** wells, 18 **P1** wells, 6 **P2** wells, 11 **P3** wells, and 40 **E** wells). Furthermore, these wells were clumped spatially as would be expected—see Figure 1c.

Making predictions:

Using the above initial spatial configuration, we ran 1000 simulations on the small lattice for 20 cycles with both a Restricted neighbourhood and an Unrestricted neighbourhood (corresponding to the number of transfers in our experiment). We measured both the average bacterial and phage density and the bacterial and phage coefficient of variation in density for each run. In Figure SIV.3 we see that the Restricted neighbourhood simulation is predicted to have significantly higher bacterial density, significantly lower phage density, and significantly lower bacteria and phage CVs than the Unrestricted neighbourhood simulation.

The predicted phage densities are quite close to the observed phage densities (do note that the average phage density in the Unrestricted treatment was predicted to be *higher* than what we found in the experimental treatment). The predicted bacterial densities are 3-4 times higher than what we observed in the experimental run. We believe that the lower bacterial densities in the experiment occurred because of the way the bacterial counts were executed: the entire metapopulation was mixed and quickly diluted before plating out the bacteria. Such mixing means that previously separated bacteria and phage would be in contact. Even though we tried to minimize the time that bacteria and phage were together before dilution, this mixing would inevitably lead to some killing of the host by the phage (incidentally, this attachment of phage should not affect the phage counts as the phage were plated before lysing would occur, thus post-mixing infection would not raise the number of plaque forming units). Such mixing also probably partially accounts for why the observed bacterial CVs were greater than those predicted. If phage hits high values when bacteria is at low densities and vice versa, most post-mixing killing of bacteria will occur when the bacteria is at low density, which will tend to lift the coefficient of variation.

Figure SIV.3

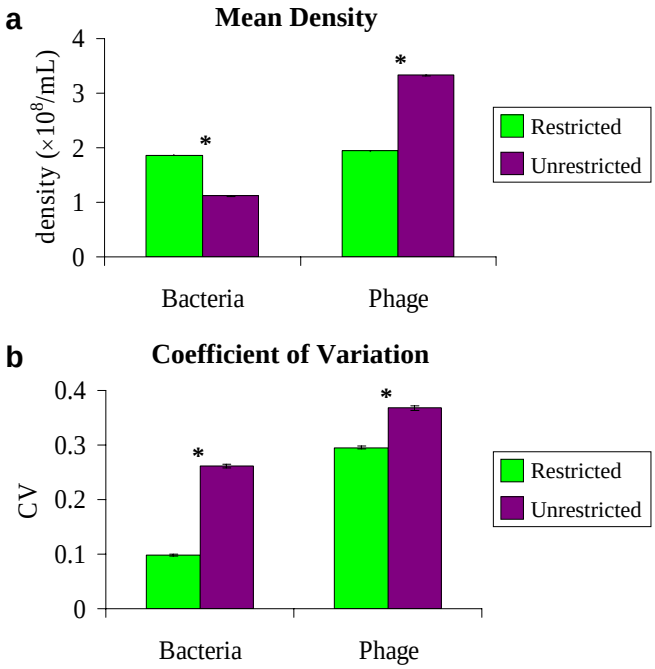

(a) The average bacteria and phage densities over 20 time steps in 1000 small lattice simulations with either a Restricted or Unrestricted neighbourhood (b) The coefficient of variation in bacteria and phage density in 1000 small lattice simulations with either a Restricted or Unrestricted neighbourhood.

V. *Evolutionary Model*

Section overview:

In this section, we extend our model to include both rapacious and prudent phage, where rapacious phage are better competitors within mixed wells and prudent phage are more productive (and thus more persistent) when alone. We describe the enlarged state space and how we incorporate mutation, competition and persistence differences between strains to arrive at a new transition matrix. This matrix is used to check our intuitions through stochastic cellular automata and configuration field approximations. We should make it clear that our goal here is not to design the most accurate model (if this was our goal, it would be best to track the densities of both phage types as continuous values, rather than discrete states). Rather, we would like to gain some knowledge of the metapopulation's behaviour given a basic trade-off between productivity and competitive ability in our phage.

Well states:

Ignoring mixed wells for the moment, we have the following well-states to consider:

1) **B** (a well filled with bacteria and a sub-critical titre of both phage types)
2) **P1** (a well filled with the highest super-critical titre of prudent phage and no bacteria)
3) **P2** (a well filled with the second highest super-critical titre of prudent phage and no bacteria)
4) **P3** (a well filled with the third highest super-critical titre of prudent phage and no bacteria)
5) **R1** (a well filled with the highest super-critical titre of rapacious phage and no bacteria)
6) **R2** (a well filled with the second highest super-critical titre of rapacious phage and no bacteria)
7) **R3** (a well filled with the third highest super-critical titre of rapacious phage and no bacteria)
8) **E** (a well filled with no bacteria and a sub-critical titre of both phage types)

We let '**P**' now stand for 'prudent phage' (as opposed to just 'phage'), whereas '**R**' stands for 'rapacious phage'. Now, if a well has both types of phage types, there are 9 possible combinations: {**P1R1**, **P1R2**, **P1R3**, **P2R1**, **P2R2**, **P2R3**, **P3R1**, **P3R2**, **P3R3**}. However, this makes the well-state transition matrix quite large (17×17). In order to reduce this matrix a bit, we make some simplifying assumptions about mutation and competition (which, as is shown below, removes 4 states from the total list). With this collection of well states, there are three processes that we must make explicit: (1) mutation, (2) competition, and (3) persistence. After spelling out our notation, we describe each below.

Notation:

We will use the following notation to represent the transition of a focal well in state **X** to state **Y**, given that a migration event occurred from a well in state **Z**:

$$\mathbf{X} \xrightarrow{\mathbf{Z}} \mathbf{Y} .$$

And we use the following notation to represent the transition of a focal well in state **X** to state **Y**, given no migration event occurred (just a dilution):

$$\mathbf{X} \longrightarrow \mathbf{Y} .$$

Mutation:

In our model, mutations in phage only occur when phage are actively replicating on their host. Further, we only allow mutation from prudent phage to rapacious phage. Specifically, we assume:

$$\mathbf{Pi} \xrightarrow{B} \mathbf{P1}, \text{ with probability } (1-\mu),$$
$$\mathbf{Pi} \xrightarrow{B} \mathbf{P1R1}, \text{ with probability } \mu,$$

where $\mathbf{i} \in \{\mathbf{1},\mathbf{2},\mathbf{3}\}$. Thus, in a well with any super-critical titre of prudent phage, if a migration event brings the bacterial host into the focal well, we assume that a mutation introducing rapacious phage can occur with probability μ (generally taken to be very small). If such a mutation occurs, the final state of the focal well is assumed to be **P1R1** (i.e., both phage types are present at high titres; thus we assume the rapacious mutant, which is the better competitor, increases in frequency within the well after the initial mutation). Note that we do not consider back mutation from rapacious phage to prudent phage (or another way to think of this is that back mutation occurs, but the superior competitive ability of rapacious types always prevents the prudent mutants from increasing in frequency within a mixed well given the addition of bacteria).

Competition:

Competition between phage types occurs only in mixed wells when fresh host cells are introduced. Here, we assume the following:

$$\mathbf{PiRj} \xrightarrow{B} \mathbf{P1R1}, \text{ with probability } (1-\beta),$$
$$\mathbf{PiRj} \xrightarrow{B} \mathbf{R1}, \text{ with probability } \beta,$$

where $\mathbf{i},\mathbf{j} \in \{\mathbf{1},\mathbf{2},\mathbf{3}\}$. The parameter β measures the probability that the rapacious phage displaces the prudent phage in a mixed well given the addition of bacterial cells. For simplicity, we assume that if the rapacious phage does not displace the prudent cohabitant, then both phage types increase to their highest titre. This assumption is a substantial simplification, as **P1R1**, **P2R2**, **P2R3**, **P3R2**, and **P3R3** have the same probability of a transition to **R1** (or **P1R1**). However, this assumption allows us to ignore four mixed well combinations (namely, **P1R2**, **P1R3**, **P2R1**, and **P3R1**). Essentially, the parameter β gives the competitive advantage of the rapacious strain.

Persistence:

The rapacious strain is less productive than the prudent strain. We capture this feature by making the rapacious strain more likely to enter the empty well state than the prudent strain. Specifically, we assume:

$$\mathbf{PiR2} \longrightarrow \mathbf{P(i+1)R3}, \text{ with probability } \pi,$$
$$\mathbf{PiR2} \longrightarrow \mathbf{P(i+1)}, \text{ with probability } 1-\pi,$$

where $\mathbf{i} \in \{\mathbf{2},\mathbf{3},\mathbf{4}\}$ and $\mathbf{Pj} \equiv \mathbf{E}$ and $\mathbf{PjRk} \equiv \mathbf{Rk}$ when $\mathbf{j} > \mathbf{3}$ and $\mathbf{k} \in \{\mathbf{2},\mathbf{3}\}$. The parameter π measures the probability that the rapacious strain will not exit the well upon dilution from the second highest

titre state (**R2**). Note that the transition $\mathbf{P2} \longrightarrow \mathbf{E}$ never occurs, whereas $\mathbf{R2} \longrightarrow \mathbf{E}$ can occur with probability $1-\pi>0$. Essentially, the parameter π gives the persistence of the rapacious strain.

Trade-off:

We assume that competitive ability and productivity trade-off (as we have empirical support for such a claim). We incorporate this feature by making β a monotonic decreasing function of π. Thus, as the rapacious strain becomes more productive/persistent (π increases), it becomes a poorer competitor (β decreases). Specifically, we assume the power function form:

$$\beta = (1-\pi)^{\gamma},$$

where γ is a parameter that controls the concavity of this trade-off (a concave trade-off requires $\gamma<1$, a linear trade-off requires $\gamma=1$, and a convex trade-off requires $\gamma>1$).

Full transition table:

Using the information above, we can construct the following transition table, where the entries are the well-states of the sources of migration that allow a focal well in the row state to transition to the column state:

	Future State												
Current state	**B**	**P1**	**P2**	**P3**	**R1**	**R2**	**R3**	**P1R1**	**P2R2**	**P3R2**	**P2R3**	**P3R3**	**E**
B	a_1	a_2			a_3			a_4					
P1		b_1	b_2					b_3	b_4		b_5		
P2		c_1	c_2	c_3				c_4	c_5	c_6		c_7	
P3		d_1	d_2	d_3		d_4	d_5	d_6	d_7			d_8	d_9
R1					e_1	e_2			e_3	e_4			
R2			f_1	f_2	f_3	f_4	f_5		f_6		f_7	f_8	f_9
R3			g_1	g_2	g_3	g_4	g_5		g_6			g_7	g_8
P1R1					h_1			h_2	h_3				
P2R2			i_1	i_2	i_3			i_4	i_5	i_6	i_7	i_8	
P3R2			j_1	j_2	j_3	j_4	j_5	j_6	j_7		j_8	j_9	j_{10}
P2R3			k_1	k_2	k_3			k_4	k_5	k_6		k_7	
P3R3			l_1	l_2	l_3	l_4	l_5	l_6	l_7			l_8	l_9
E	m_1		m_2	m_3		m_4	m_5		m_6			m_7	m_8

Each of the entries in the above table is actually a collection of well-states that produce the relevant transition. For instance, if entry $\boldsymbol{n_i} \equiv \{\varnothing, \mathbf{W}, \mathbf{Z}(p)\}$ is found in row **X** and column **Y**, this means that the following transitions occur:

$$\mathbf{X} \longrightarrow \mathbf{Y},$$
$$\mathbf{X} \xrightarrow{\mathbf{W}} \mathbf{Y},$$
$$\mathbf{X} \xrightarrow{\mathbf{Z}} \mathbf{Y}, \text{ with probability } p.$$

Thus, the symbol ∅ refers to a straight dilution without a migration event and **Z**(p) refers to a transition that occurs with probability p when the source well of migration is in state **Z**. The entries of the table are the following sets:

$\boldsymbol{a_1}$≡{∅, **B**, **E**}
$\boldsymbol{a_2}$≡{**P1**(1−μ), **P2**(1−μ), **P3**(1−μ)}
$\boldsymbol{a_3}$≡{**R1**, **R2**, **R3**, **P1R1**(β), **P2R2**(β), **P2R3**(β), **P3R2**(β), **P3R3**(β)}
$\boldsymbol{a_4}$≡{**P1**(μ), **P2**(μ), **P3**(μ), **P1R1**(1−β), **P2R2**(1−β), **P2R3**(1−β), **P3R2**(1−β), **P3R3**(1−β)}
$\boldsymbol{b_1}$≡{**B**(1−μ)}
$\boldsymbol{b_2}$≡{∅, **P1**, **P2**, **P3**, **R3**, **P2R3**, **P3R3**, **E**, **R2**(1−π), **P2R2**(1−π), **P3R2**(1−π)}
$\boldsymbol{b_3}$≡{**B**(μ)}
$\boldsymbol{b_4}$≡{**R1**, **P1R1**}
$\boldsymbol{b_5}$≡{**R2**(π), **P2R2**(π), **P3R2**(π)}
$\boldsymbol{c_1}$≡{**B**(1−μ)}
$\boldsymbol{c_2}$≡{**P1**}
$\boldsymbol{c_3}$≡{∅, **P2**, **P3**, **R3**, **P2R3**, **P3R3**, **E**, **R2**(1−π), **P2R2**(1−π), **P3R2**(1−π)}
$\boldsymbol{c_4}$≡{**B**(μ)}
$\boldsymbol{c_5}$≡{**P1R1**}
$\boldsymbol{c_6}$≡{**R1**}
$\boldsymbol{c_7}$≡{**R2**(π), **P2R2**(π), **P3R2**(π)}
$\boldsymbol{d_1}$≡{**B**(1−μ)}
$\boldsymbol{d_2}$≡{**P1**}
$\boldsymbol{d_3}$≡{**P2**, **P2R3**, **P2R2**(1−π)}
$\boldsymbol{d_4}$≡{**R1**}
$\boldsymbol{d_5}$≡{**R2**(π), **P3R2**(π),}
$\boldsymbol{d_6}$≡{**B**(μ)}
$\boldsymbol{d_7}$≡{**P1R1**}
$\boldsymbol{d_8}$≡{**P2R2**(π)}
$\boldsymbol{d_9}$≡{∅, **P3**, **R3**, **P3R3**, **E**, **R2**(1−π), **P3R2**(1−π)}
$\boldsymbol{e_1}$≡{**B**}
$\boldsymbol{e_2}$≡{∅, **P3**, **R1**, **R2**, **R3**, **P3R2**, **P3R3**, **E**}
$\boldsymbol{e_3}$≡{**P1**, **P1R1**}
$\boldsymbol{e_4}$≡{**P2**, **P2R2**, **P2R3**}
$\boldsymbol{f_1}$≡{**P1**(1−π)}
$\boldsymbol{f_2}$≡{**P2**(1−π), **P2R3**(1−π), **P2R2**((1−π)^2)}
$\boldsymbol{f_3}$≡{**B**}
$\boldsymbol{f_4}$≡{**R1**}
$\boldsymbol{f_5}$≡{∅(π), **P3**(π), **R3**(π), **P3R3**(π), **E**(π), **R2**(1−(1−π)^2), **P3R2**(1−(1−π)^2)}
$\boldsymbol{f_6}$≡{**P1R1**}
$\boldsymbol{f_7}$≡{**P1**(π)}
$\boldsymbol{f_8}$≡{**P2**(π), **P2R3**(π), **P2R2**(1−(1−π)^2)}
$\boldsymbol{f_9}$≡{∅(1−π), **P3**(1−π), **R3**(1−π), **P3R3**(1−π), **E**(1−π), **R2**((1−π)^2), **P3R2**((1−π)^2)}
$\boldsymbol{g_1}$≡{**P1**}
$\boldsymbol{g_2}$≡{**P2**, **P2R3**, **P2R2**(1−π)}

$\boldsymbol{g_3}\equiv\{\mathbf{B}\}$
$\boldsymbol{g_4}\equiv\{\mathbf{R1}\}$
$\boldsymbol{g_5}\equiv\{\mathbf{R2}(\pi), \mathbf{P3R2}(\pi)\}$
$\boldsymbol{g_6}\equiv\{\mathbf{P1R1}\}$
$\boldsymbol{g_7}\equiv\{\mathbf{P2R2}(\pi)\}$
$\boldsymbol{g_8}\equiv\{\varnothing, \mathbf{P3}, \mathbf{R3}, \mathbf{P3R3}, \mathbf{E}, \mathbf{R2}(1-\pi), \mathbf{P3R2}(1-\pi)\}$
$\boldsymbol{h_1}\equiv\{\mathbf{B}(\beta)\}$
$\boldsymbol{h_2}\equiv\{\mathbf{B}(1-\beta)\}$
$\boldsymbol{h_3}\equiv\{\varnothing, \mathbf{P1}, \mathbf{P2}, \mathbf{P3}, \mathbf{R1}, \mathbf{R2}, \mathbf{R3}, \mathbf{P1R1}, \mathbf{P2R2}, \mathbf{P3R2}, \mathbf{P2R3}, \mathbf{P3R3}, \mathbf{E}\}$
$\boldsymbol{i_1}\equiv\{\mathbf{P1}(1-\pi)\}$
$\boldsymbol{i_2}\equiv\{\varnothing(1-\pi), \mathbf{P2}(1-\pi), \mathbf{P3}(1-\pi), \mathbf{R3}(1-\pi), \mathbf{P2R3}(1-\pi), \mathbf{P3R3}(1-\pi), \mathbf{E}(1-\pi), \mathbf{R2}((1-\pi)^2),$
$\mathbf{P2R2}((1-\pi)^2), \mathbf{P3R2}((1-\pi)^2)\}$
$\boldsymbol{i_3}\equiv\{\mathbf{B}(\beta)\}$
$\boldsymbol{i_4}\equiv\{\mathbf{B}(1-\beta)\}$
$\boldsymbol{i_5}\equiv\{\mathbf{P1R1}\}$
$\boldsymbol{i_6}\equiv\{\mathbf{R1}\}$
$\boldsymbol{i_7}\equiv\{\mathbf{P1}(\pi)\}$
$\boldsymbol{i_8}\equiv\{\varnothing(\pi), \mathbf{P2}(\pi), \mathbf{P3}(\pi), \mathbf{R3}(\pi), \mathbf{P2R3}(\pi), \mathbf{P3R3}(\pi), \mathbf{E}(\pi), \mathbf{R2}(1-(1-\pi)^2),$
$\mathbf{P2R2}(1-(1-\pi)^2), \mathbf{P3R2}(1-(1-\pi)^2)\}$
$\boldsymbol{j_1}\equiv\{\mathbf{P1}(1-\pi)\}$
$\boldsymbol{j_2}\equiv\{\mathbf{P2}(1-\pi), \mathbf{P2R3}(1-\pi), \mathbf{P2R2}((1-\pi)^2)\}$
$\boldsymbol{j_3}\equiv\{\mathbf{B}(\beta)\}$
$\boldsymbol{j_4}\equiv\{\mathbf{R1}\}$
$\boldsymbol{j_5}\equiv\{\varnothing(\pi), \mathbf{P3}(\pi), \mathbf{R3}(\pi), \mathbf{P3R3}(\pi), \mathbf{E}(\pi), \mathbf{R2}(1-(1-\pi)^2), \mathbf{P3R2}(1-(1-\pi)^2)\}$
$\boldsymbol{j_6}\equiv\{\mathbf{B}(1-\beta)\}$
$\boldsymbol{j_7}\equiv\{\mathbf{P1R1}\}$
$\boldsymbol{j_8}\equiv\{\mathbf{P1}(\pi)\}$
$\boldsymbol{j_9}\equiv\{\mathbf{P2}(\pi), \mathbf{P2R3}(\pi), \mathbf{P2R2}(1-(1-\pi)^2)\}$
$\boldsymbol{j_{10}}\equiv\{\varnothing(1-\pi), \mathbf{P3}(1-\pi), \mathbf{R3}(1-\pi), \mathbf{P3R3}(1-\pi), \mathbf{E}(1-\pi), \mathbf{R2}((1-\pi)^2), \mathbf{P3R2}((1-\pi)^2)\}$
$\boldsymbol{k_1}\equiv\{\mathbf{P1}\}$
$\boldsymbol{k_2}\equiv\{\varnothing, \mathbf{P2}, \mathbf{P3}, \mathbf{R3}, \mathbf{P2R3}, \mathbf{P3R3}, \mathbf{E}, \mathbf{R2}(1-\pi), \mathbf{P2R2}(1-\pi), \mathbf{P3R2}(1-\pi)\}$
$\boldsymbol{k_3}\equiv\{\mathbf{B}(\beta)\}$
$\boldsymbol{k_4}\equiv\{\mathbf{B}(1-\beta)\}$
$\boldsymbol{k_5}\equiv\{\mathbf{P1R1}\}$
$\boldsymbol{k_6}\equiv\{\mathbf{R1}\}$
$\boldsymbol{k_7}\equiv\{\mathbf{R2}(\pi), \mathbf{P2R2}(\pi), \mathbf{P3R2}(\pi)\}$
$\boldsymbol{l_1}\equiv\{\mathbf{P1}\}$
$\boldsymbol{l_2}\equiv\{\mathbf{P2}, \mathbf{P2R3}, \mathbf{P2R2}(1-\pi)\}$
$\boldsymbol{l_3}\equiv\{\mathbf{B}(\beta)\}$
$\boldsymbol{l_4}\equiv\{\mathbf{R1}\}$
$\boldsymbol{l_5}\equiv\{\mathbf{R2}(\pi), \mathbf{P3R2}(\pi)\}$
$\boldsymbol{l_6}\equiv\{\mathbf{B}(1-\beta)\}$
$\boldsymbol{l_7}\equiv\{\mathbf{P1R1}\}$
$\boldsymbol{l_8}\equiv\{\mathbf{P2R2}(\pi)\}$

$\boldsymbol{l_9}\equiv\{\varnothing,$ **P3**, **R3**, **P3R3**, **E**, **R2**$(1-\pi)$, **P3R2**$(1-\pi)\}$
$\boldsymbol{m_1}\equiv\{$**B**$\}$
$\boldsymbol{m_2}\equiv\{$**P1**$\}$
$\boldsymbol{m_3}\equiv\{$**P2**, **P2R3**, **P2R2**$(1-\pi)\}$
$\boldsymbol{m_4}\equiv\{$**R1**$\}$
$\boldsymbol{m_5}\equiv\{$**R2**(π), **P3R2**$(\pi)\}$
$\boldsymbol{m_6}\equiv\{$**P1R1**$\}$
$\boldsymbol{m_7}\equiv\{$**P2R2**$(\pi)\}$
$\boldsymbol{m_8}\equiv\{\varnothing,$ **P3**, **R3**, **P3R3**, **E**, **R2**$(1-\pi)$, **P3R2**$(1-\pi)\}$

Configuration field approach:

In order to use the configuration field approach, we consider the following vector:

$$\mathbf{x}_t = \left\langle B_t, P1_t, P2_t, P3_t, R1_t, R2_t, R3_t, P1R1_t, P2R2_t, P3R2_t, P2R3_t, P3R3_t, E_t \right\rangle,$$

which gives the frequencies of each of the 13 well states at time *t*. Given an infinite number of wells, a global migration neighbourhood and a migration probability of *m*, the dynamics of **x** are given by:

$$\mathbf{x}_{t+1} = \mathbf{x}_t \mathbf{M}_t,$$

with

$$\mathbf{M}_t = \begin{bmatrix}
a_1 & a_2 & 0 & 0 & a_3 & 0 & 0 & a_4 & 0 & 0 & 0 & 0 & 0 \\
0 & b_1 & b_2 & 0 & 0 & 0 & 0 & b_3 & b_4 & 0 & b_5 & 0 & 0 \\
0 & c_1 & c_2 & c_3 & 0 & 0 & 0 & c_4 & c_5 & c_6 & 0 & c_7 & 0 \\
0 & d_1 & d_2 & d_3 & 0 & d_4 & d_5 & d_6 & d_7 & 0 & 0 & d_8 & d_9 \\
0 & 0 & 0 & 0 & e_1 & e_2 & 0 & 0 & e_3 & e_4 & 0 & 0 & 0 \\
0 & 0 & f_1 & f_2 & f_3 & f_4 & f_5 & 0 & f_6 & 0 & f_7 & f_8 & f_9 \\
0 & 0 & g_1 & g_2 & g_3 & g_4 & g_5 & 0 & g_6 & 0 & 0 & g_7 & g_8 \\
0 & 0 & 0 & 0 & h_1 & 0 & 0 & h_2 & h_3 & 0 & 0 & 0 & 0 \\
0 & 0 & i_1 & i_2 & i_3 & 0 & 0 & i_4 & i_5 & i_6 & i_7 & i_8 & 0 \\
0 & 0 & j_1 & j_2 & j_3 & j_4 & j_5 & j_6 & j_7 & 0 & j_8 & j_9 & j_{10} \\
0 & 0 & k_1 & k_2 & k_3 & 0 & 0 & k_4 & k_5 & k_6 & 0 & k_7 & 0 \\
0 & 0 & l_1 & l_2 & l_3 & l_4 & l_5 & l_6 & l_7 & 0 & 0 & l_8 & l_9 \\
m_1 & 0 & m_2 & m_3 & 0 & m_4 & m_5 & 0 & m_6 & 0 & 0 & m_7 & m_8
\end{bmatrix},$$

where (below we let λ=1−π)

$$a_1 = (1-m) + m(E_t + B_t)$$
$$a_2 = m(1-\mu)(P1_t + P2_t + P3_t)$$
$$a_3 = m(R1_t + R2_t + R3_t + \beta(P1R1_t + P2R2_t + P2R3_t + P3R2_t + P3R3_t))$$
$$a_4 = m(\mu(P1_t + P2_t + P3_t) + (1-\beta)(P1R1_t + P2R2_t + P2R3_t + P3R2_t + P3R3_t))$$
$$b_1 = m(1-\mu)B_t$$
$$b_2 = (1-m) + m(P1_t + P2_t + P3_t + R3_t + P2R3_t + P3R3_t + E_t + \lambda(R2_t + P2R2_t + P3R2_t))$$
$$b_3 = m\mu B_t$$
$$b_4 = m(R1_t + P1R1_t)$$
$$b_5 = m(1-\lambda)(R2_t + P2R2_t + P3R2_t)$$
$$c_1 = m(1-\mu)B_t$$
$$c_2 = mP1_t$$
$$c_3 = (1-m) + m(P2_t + P3_t + R3_t + P2R3_t + P3R3_t + E_t + \lambda(R2_t + P2R2_t + P3R2_t))$$
$$c_4 = m\mu B_t$$
$$c_5 = mP1R1_t$$
$$c_6 = mR1_t$$
$$c_7 = m(1-\lambda)(R2_t + P2R2_t + P3R2_t)$$
$$d_1 = m(1-\mu)B_t$$
$$d_2 = mP1_t$$
$$d_3 = m(P2_t + P2R3_t + \lambda P2R2_t)$$
$$d_4 = mR1_t$$
$$d_5 = m(1-\lambda)(R2_t + P3R2_t)$$
$$d_6 = m\mu B_t$$
$$d_7 = mP1R1_t$$
$$d_8 = m(1-\lambda)P2R2_t$$
$$d_9 = (1-m) + m(P3_t + R3_t + P3R3_t + E_t + \lambda(R2_t + P3R2_t))$$
$$e_1 = mB_t$$
$$e_2 = (1-m) + m(P3_t + R1_t + R2_t + R3_t + P3R2_t + P3R3_t + E_t)$$
$$e_3 = m(P1_t + P1R1_t)$$
$$e_4 = m(P2_t + P2R2_t + P2R3_t)$$
$$f_1 = m\lambda P1_t$$
$$f_2 = m(\lambda(P2_t + P2R3_t) + \lambda^2 P2R2_t)$$
$$f_3 = mB_t$$
$$f_4 = mR1_t$$
$$f_5 = (1-m)(1-\lambda) + m((1-\lambda)(P3_t + R3_t + P3R3_t + E_t) + (1-\lambda^2)(R2_t + P3R2_t))$$
$$f_6 = mP1R1_t$$
$$f_7 = m(1-\lambda)P1_t$$

$$f_8 = m((1-\lambda)(P2_t + P2R3_t) + (1-\lambda^2)P2R2_t)$$
$$f_9 = (1-m)\lambda + m(\lambda(P3_t + R3_t + P3R3_t + E_t) + \lambda^2(R2_t + P3R2_t))$$
$$g_1 = mP1_t$$
$$g_2 = m(P2_t + P2R3_t + \lambda P2R2_t)$$
$$g_3 = mB_t$$
$$g_4 = mR1_t$$
$$g_5 = m((1-\lambda)(R2_t + P3R2_t))$$
$$g_6 = mP1R1_t$$
$$g_7 = m(1-\lambda)P2R2_t$$
$$g_8 = (1-m) + m(P3_t + R3_t + P3R3_t + E_t + \lambda(R2_t + P3R2_t))$$
$$h_1 = m\beta B_t$$
$$h_2 = m(1-\beta)B_t$$
$$h_3 = (1-m) + m(P1_t + P2_t + P3_t + R1_t + R2_t + R3_t + P1R1_t + P2R2_t + P3R2_t + P2R3_t + P3R3_t + E_t)$$
$$i_1 = m\lambda P1_t$$
$$i_2 = (1-m)\lambda + m(\lambda(P2_t + P3_t + R3_t + P2R3_t + P3R3_t + E_t) + \lambda^2(R2_t + P2R2_t + P3R2_t))$$
$$i_3 = m\beta B_t$$
$$i_4 = m(1-\beta)B_t$$
$$i_5 = mP1R1_t$$
$$i_6 = mR1_t$$
$$i_7 = m(1-\lambda)P1_t$$
$$i_8 = (1-m)(1-\lambda) + m((1-\lambda)(P2_t + P3_t + R3_t + P2R3_t + P3R3_t + E_t) + (1-\lambda^2)(R2_t + P2R2_t + P3R2_t))$$
$$j_1 = m\lambda P1_t$$
$$j_2 = m(\lambda(P2_t + P2R3_t) + \lambda^2 P2R2_t)$$
$$j_3 = m\beta B_t$$
$$j_4 = mR1_t$$
$$j_5 = (1-m)(1-\lambda) + m((1-\lambda)(P3_t + R3_t + P3R3_t + E_t) + (1-\lambda^2)(R2_t + P3R2_t))$$
$$j_6 = m(1-\beta)B_t$$
$$j_7 = mP1R1_t$$
$$j_8 = m(1-\lambda)P1_t$$
$$j_9 = m((1-\lambda)(P2_t + P2R3_t) + (1-\lambda^2)P2R2_t)$$
$$j_{10} = (1-m)\lambda + m(\lambda(P3_t + R3_t + P3R3_t + E_t) + \lambda^2(R2_t + P3R2_t))$$
$$k_1 = mP1_t$$
$$k_2 = (1-m) + m(P2_t + P3_t + R3_t + P2R3_t + P3R3_t + E_t + \lambda(R2_t + P2R2_t + P3R2_t))$$
$$k_3 = m\beta B_t$$
$$k_4 = m(1-\beta)B_t$$
$$k_5 = mP1R1_t$$

$$k_6 = mR1_t$$
$$k_7 = m(1-\lambda)(R2_t + P2R2_t + P3R2_t)$$
$$l_1 = mP1_t$$
$$l_2 = m(P2_t + P2R3_t + \lambda P2R2_t)$$
$$l_3 = m\beta B_t$$
$$l_4 = mR1_t$$
$$l_5 = m(1-\lambda)(R2_t + P3R2_t)$$
$$l_6 = m(1-\beta)B_t$$
$$l_7 = mP1R1_t$$
$$l_8 = m(1-\lambda)P2R2_t$$
$$l_9 = (1-m) + m(P3_t + R3_t + P3R3_t + E_t + \lambda(R2_t + P3R2_t))$$
$$m_1 = mB_t$$
$$m_2 = mP1_t$$
$$m_3 = m(P2_t + P2R3_t + \lambda P2R2_t)$$
$$m_4 = mR1_t$$
$$m_5 = m(1-\lambda)(R2_t + P3R2_t)$$
$$m_6 = mP1R1_t$$
$$m_7 = m(1-\lambda)P2R2_t$$
$$m_8 = (1-m) + m(P3_t + R3_t + P3R3_t + E_t + \lambda(R2_t + P3R2_t))$$

Again, $\mathbf{M}_t$ is not a constant matrix, but depends on $\mathbf{x}_t$. Let the (x,y) entry of $\mathbf{M}_t$ be given by s_{xy}. We have

$$\sum_{y=1}^{13} s_{xy} = 1,$$

for all $x \in \{1,2,3,\ldots 13\}$. That is, $\mathbf{M}_t$ is a stochastic matrix—all matrix entries in the same row have the same head letter, thus summing over a letter should always give unity (e.g., $a_1 + a_2 + a_3 + a_4 = 1$). The configuration field approximation is achieved by numerically iterating the non-linear Markov chain.

In Figure SV.1, we see the configuration field approximation that corresponds to Figure 3a (m=0.45, π=0.87, γ=0.1, and μ=0.001). In this case, the rapacious phage drives the prudent phage to extinction.

Using the full transition table above, we can also run cellular automata with both Restricted and Unrestricted neighbourhoods (e.g., Figure 3). For large lattice sizes, the dynamics of the Unrestricted neighbourhood cellular automaton corresponds to the configuration field approximation, whereas the dynamics of Restricted neighbourhood cellular automaton often deviates.

Figure SV.1: Evolutionary Configuration Field Approximation

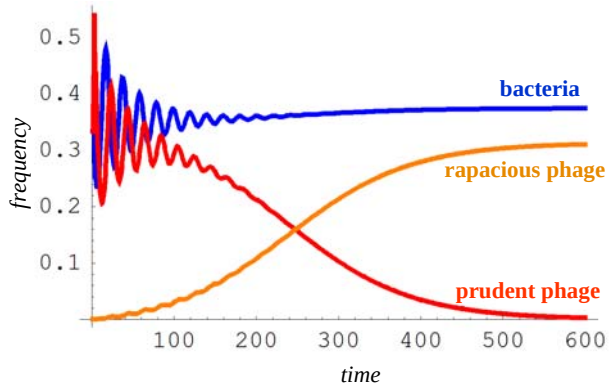

The dynamics predicted by the configuration field approximation incorporating evolution. Like the stochastic cellular automata with unrestricted migration, the rapacious phage displace the prudent phage.

In Figure SV.2, we compare the configuration field approximation to cellular automata over the same parameter search as that illustrated in Figure 3c. There is a close correspondence between the Unrestricted simulation and the configuration field approximation, whereas rapacious phage do poorly under nearly all parameters with restricted migration.

Figure SV.2

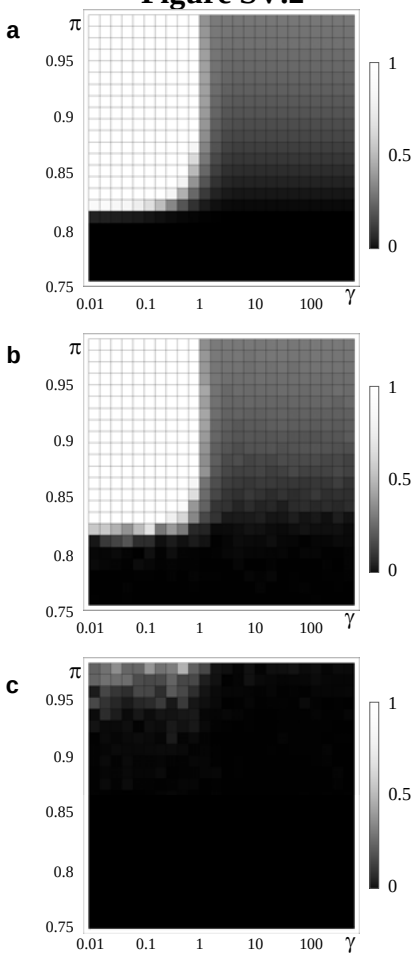

The frequency of rapacious phage after 3000 cycles is shown on a greyscale for a number of different parameter combinations (for all plots, m=0.45 and γ=0.1). (a) A parameter search using the configuration field approximation. (b) A parameter search using stochastic cellular automata with unrestricted migration. (c) A parameter search using stochastic cellular automata with restricted migration. (For each parameter search using cellular automata, each square is the average final rapacious frequency over five simulation runs).